Dual Tuning of Ultra-thin α-$Co(OH)_2$ Nanosheets by Solvent Engineering and Coordination Competition for Efficient Oxygen Evolution

Zuozhong Liang,[a] Chaochao Zhang,[a] Yang Xu,[a] Wei Zhang,[a] Haoquan Zheng,[a] and Rui Cao*[a, b]*

[a] Key Laboratory of Applied Surface and Colloid Chemistry, Ministry of Education, School of Chemistry and Chemical Engineering, Shaanxi Normal University, Xi'an, 710119, China

[b] Department of Chemistry, Renmin University of China, Beijing, 100872, China.

Corresponding Author

E-mail: zhenghaoquan@snnu.edu.cn; ruicao@ruc.edu.cn.

Number of pages: 31

Number of figures: 30

Number of tables: 0

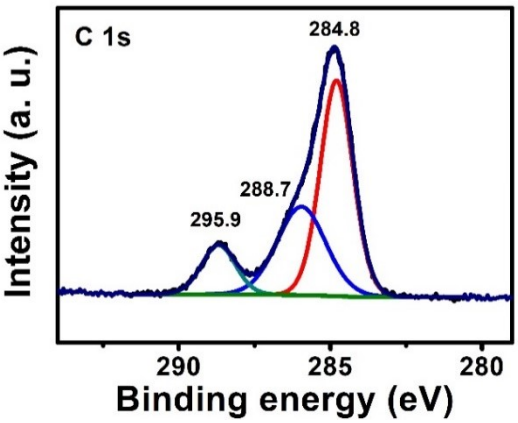

Figure S1. The high-resolution C 1s XPS spectrum

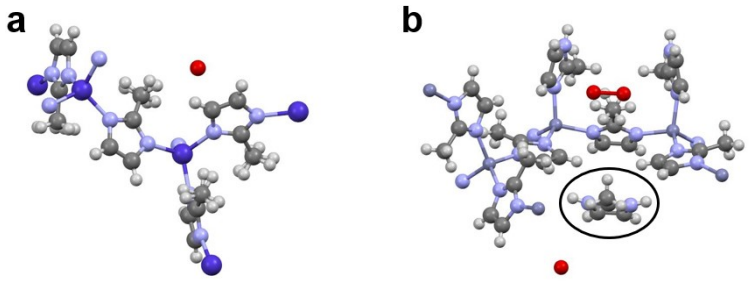

Figure S2. Crystal structures of ZIF-67 (a) and ZIF-L (b).

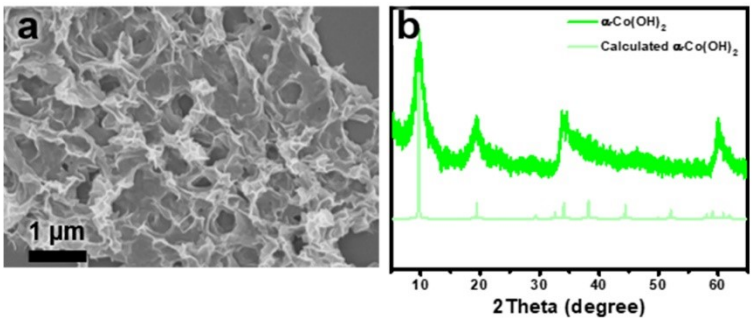

Figure S3. SEM image (a) and the corresponding XRD pattern (b) of the α-$Co(OH)_2$ obtained by dissolving $Co(NO_3)_2$ and 2-MI in methanol and water, respectively. The calculated XRD pattern of α-$Co(OH)_2$ is shown in Figure S3a_1.

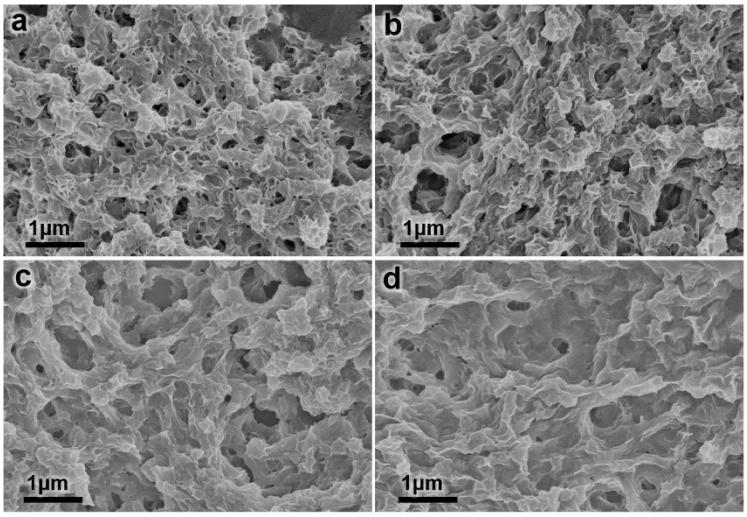

Figure S4. SEM images of the as-prepared products without aging (a) and with different aging time (b: 1h; c: 3h: d: 9h)

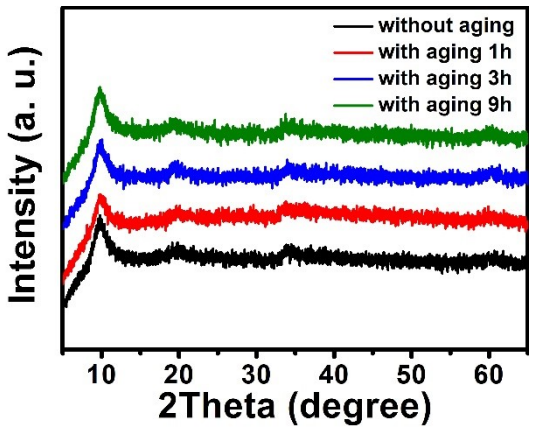

Figure S5. XRD patterns of the as-prepared products without aging and with different aging time

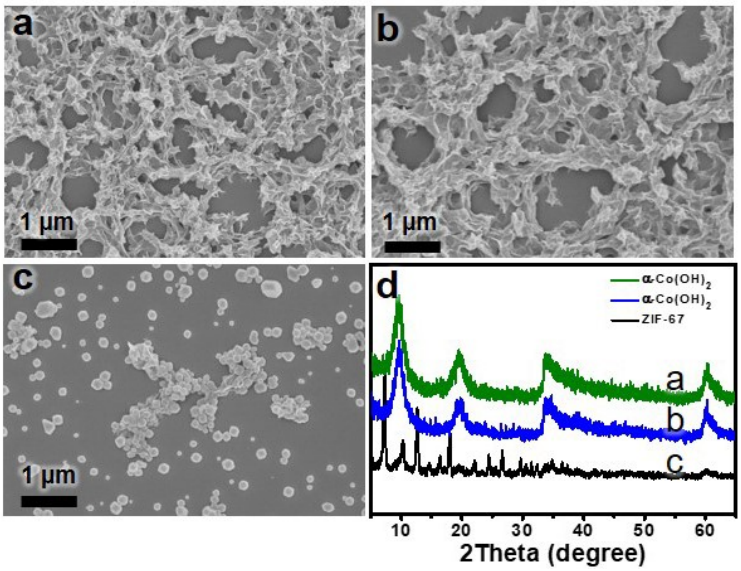

Figure S6. SEM images (a-c) and experimental XRD patterns (d) of as-prepared products with different molar ratio of Co/2-MI (a-1:1, b-1:3, and c-1:4).

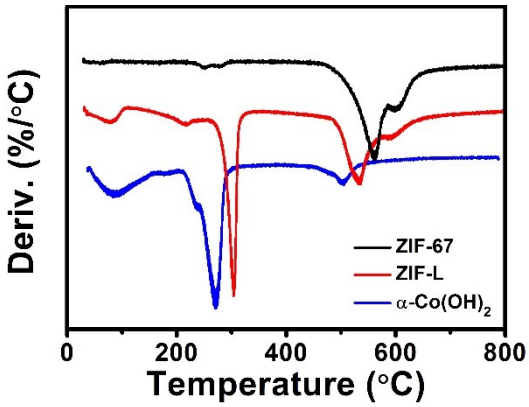

Figure S7. The differential thermal gravity (DTG) curves of the as-prepared ZIF-67, ZIF-L, and α-$Co(OH)_2$.

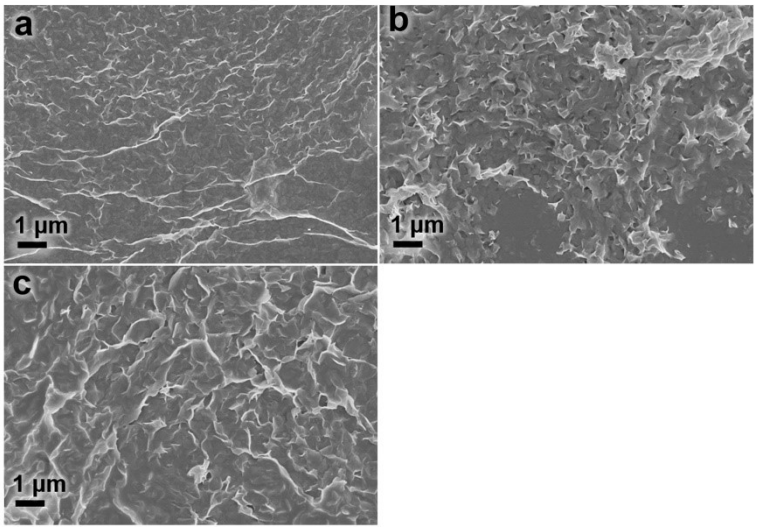

Figure S8. SEM images of the as-prepared products with different imidazole (a: 2-ethylimidazole; b: 2-propylimidazole; c: 2-buthylimidazole)

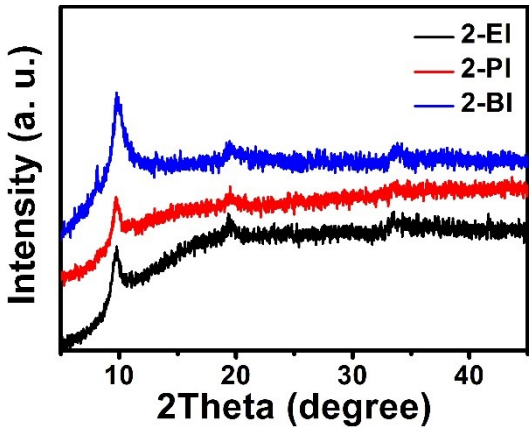

Figure S9. XRD patterns of the as-prepared products with different imidazole (2-ethylimidazole (2-EI); 2-propylimidazole (2-PI); 2-buthylimidazole (2-BI))

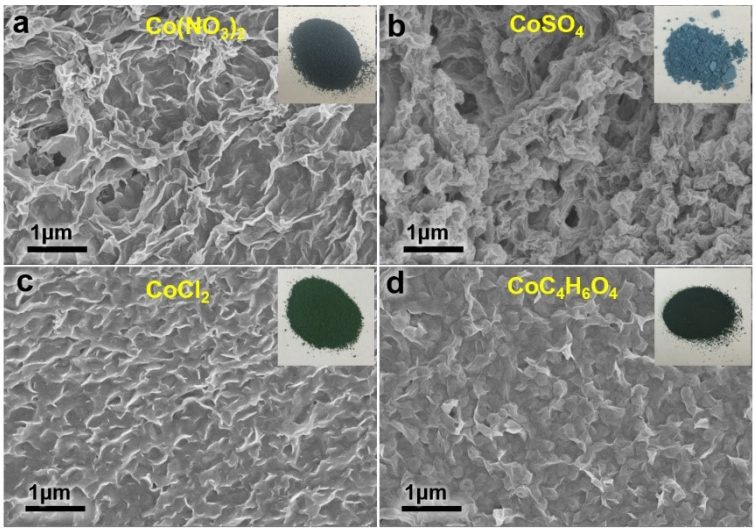

Figure S10. SEM images of the as-prepared products with different Co salts (a: $Co(NO_3)_2$; b: $CoSO_4$; c: $CoCl_2$; d: $CoC_4H_6O_4$)

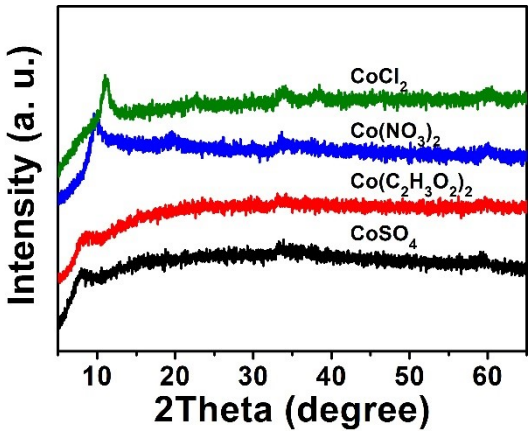

Figure S11. XRD patterns of the as-prepared products with different Co salts

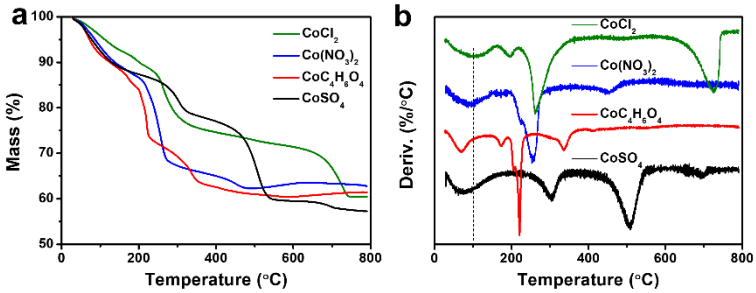

Figure S12. TGA curves (a) and corresponding DTG curves (b) of $Co(OH)_2$ nanosheets prepared with different salts

The decreased temperature of the water removal from $CoCl_2$ to $Co(NO_3)_2$ to $CoC_4H_6O_4$ to $CoSO_4$ confirms the increased distance between layers. This is because the water molecules evaporate quickly when located in nanosheets with larger layer distance. The different decomposition temperature for the as-prepared $Co(OH)_2$ nanosheets further confirms the existence of counterbalance anions between layers.

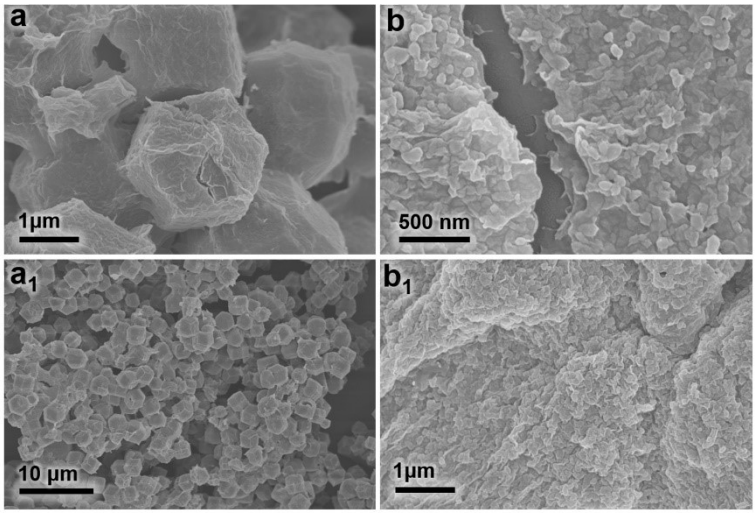

Figure S13. SEM images of the as-prepared materials dispersing the ZIF-67 (a, a_1) and ZIF-L (b, b_1) in water/methanol mixed solvent.

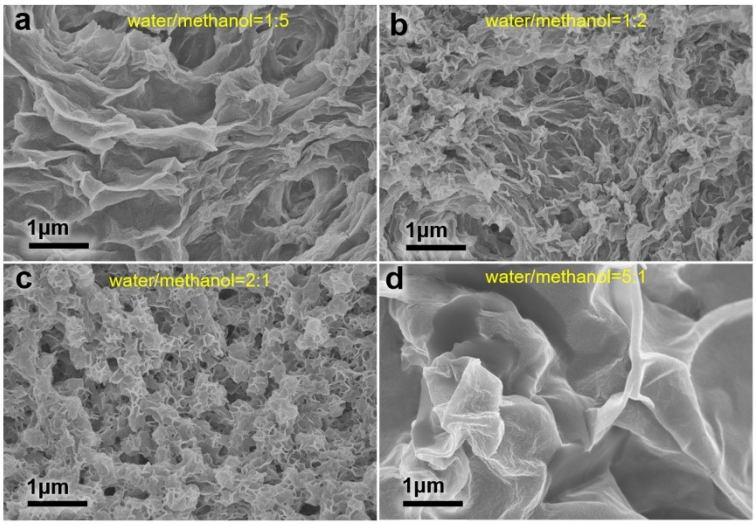

Figure S14. SEM images of the as-prepared products with different amount of solvents

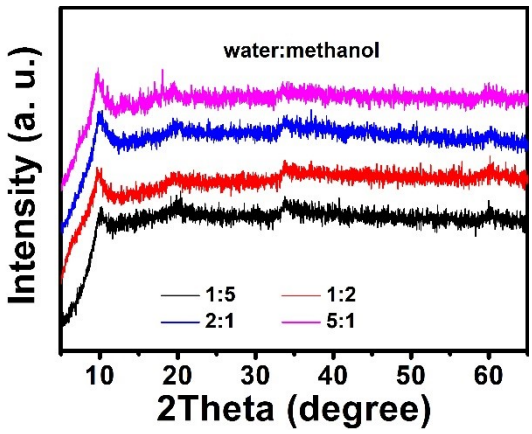

Figure S15. XRD patterns of the as-prepared products with different amount of solvents

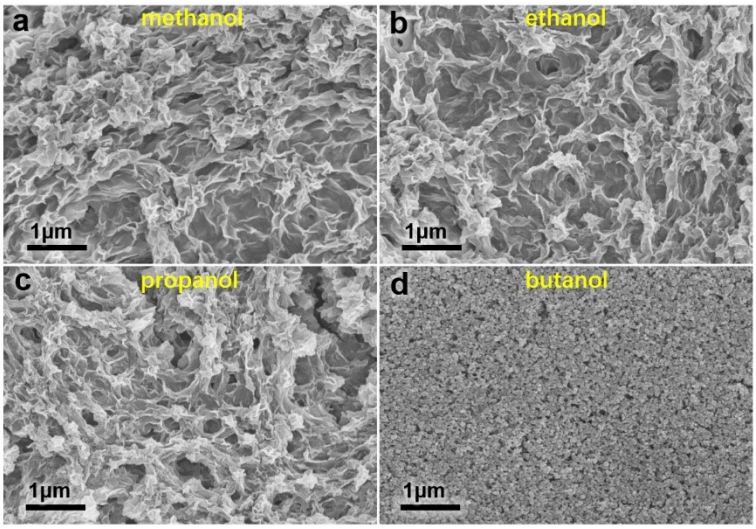

Figure S16. SEM images of the as-prepared products with different solvents (a: methanol; b: ethanol; c: propanol; d: butanol)

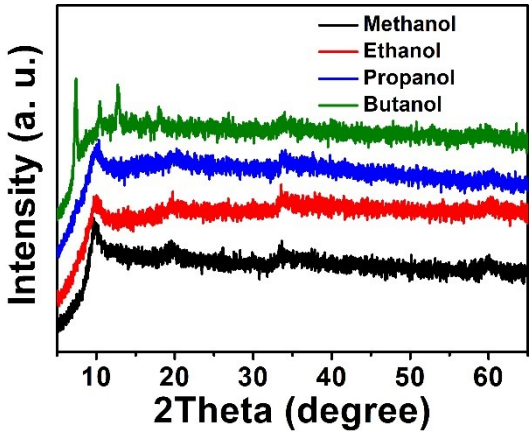

Figure S17. XRD patterns of the as-prepared products with different solvents (methanol, ethanol, propanol, and butanol)

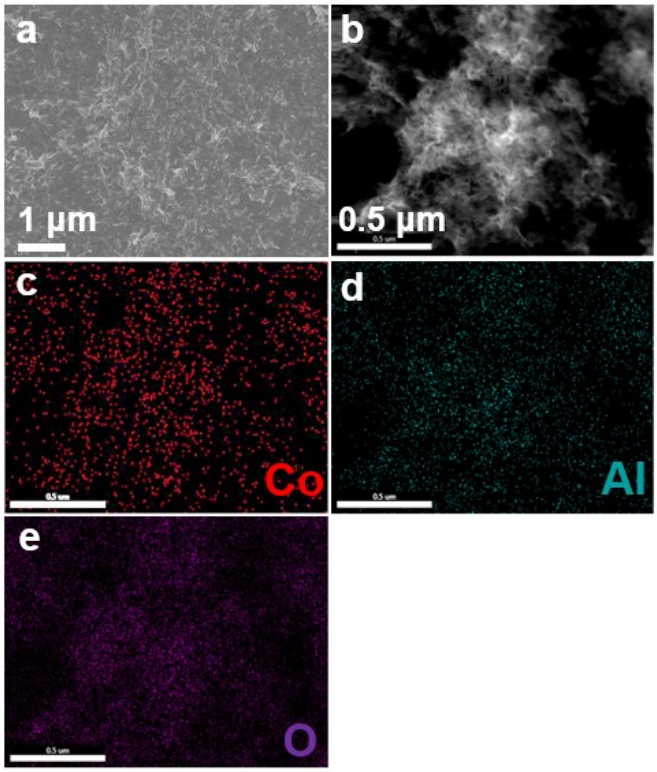

Figure S18. The SEM image (a), HAADF-STEM image (b) and the elemental mapping images (c-e) of the as-prepared Al-Co nanosheets.

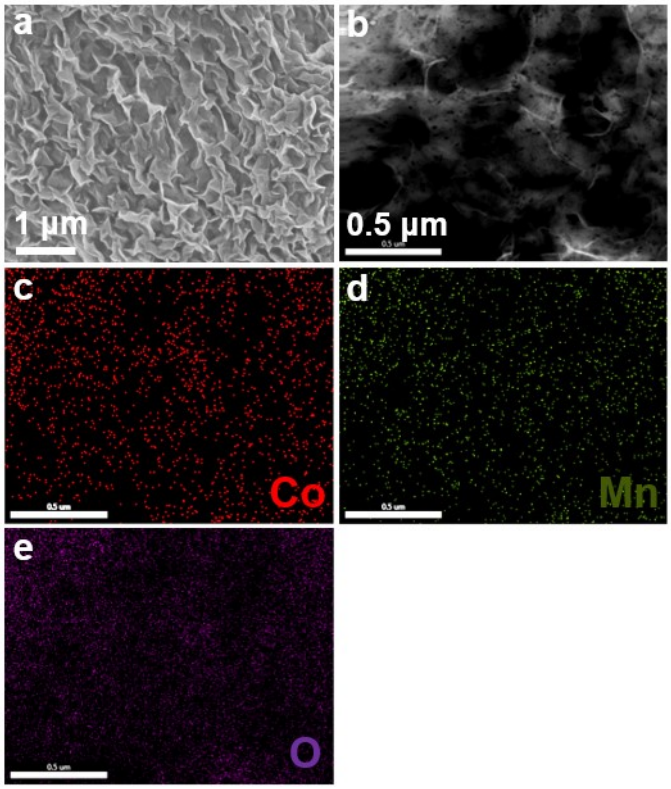

Figure S19. The SEM image (a), HAADF-STEM image (b) and the elemental mapping images (c-e) of the as-prepared Mn-Co nanosheets.

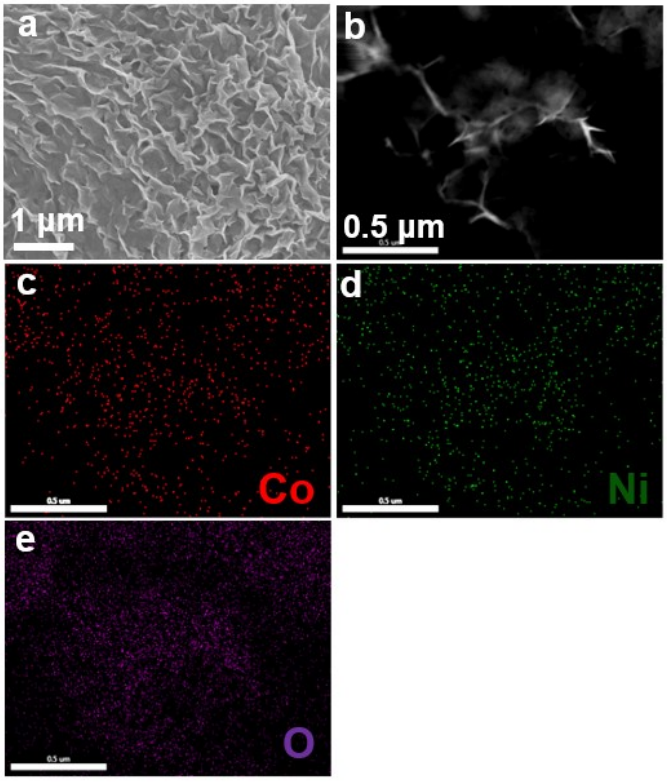

Figure S20. The SEM image (a), HAADF-STEM image (b) and the elemental mapping images (c-e) of the as-prepared Ni-Co nanosheets.

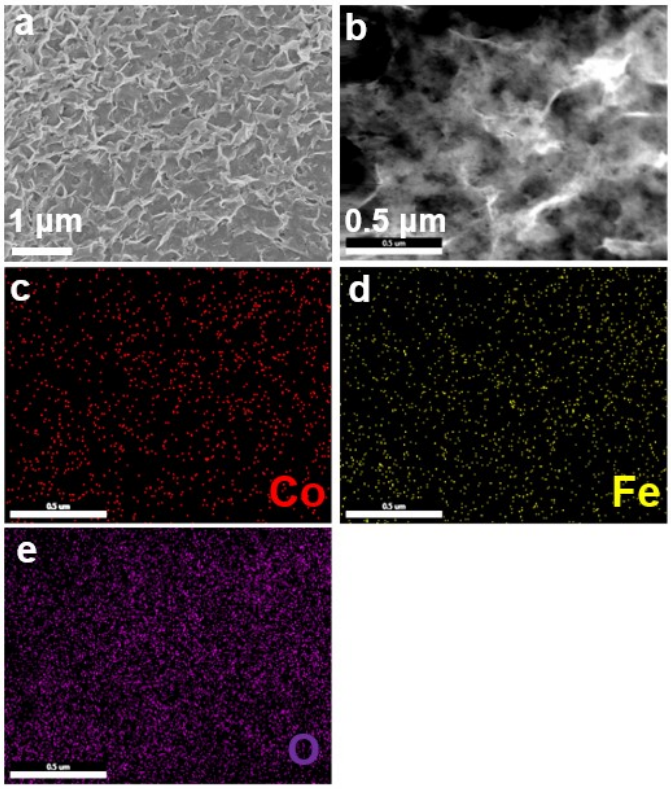

Figure S21. The SEM image (a), HAADF-STEM image (b) and the elemental mapping images (c-e) of the as-prepared Fe-Co nanosheets.

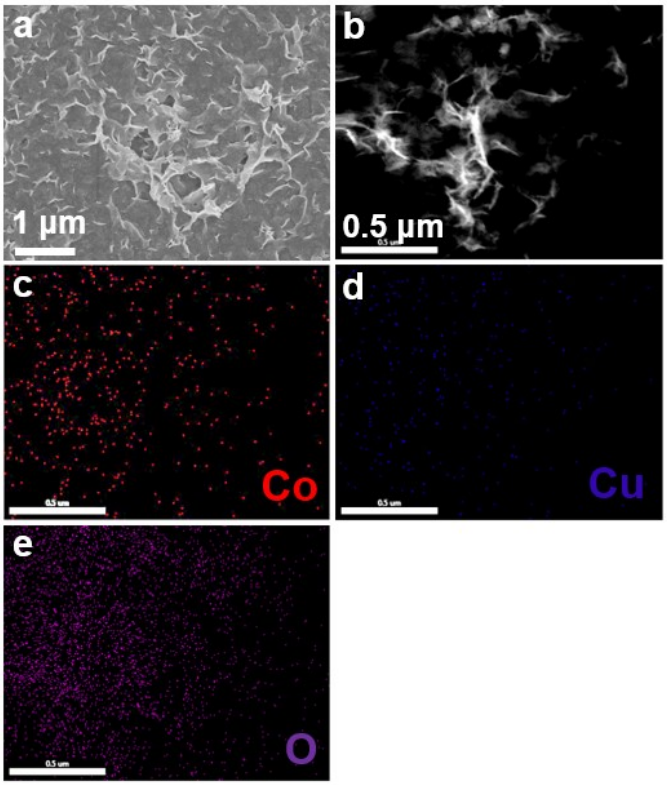

Figure S22. The SEM image (a), HAADF-STEM image (b) and the elemental mapping images (c-e) of the as-prepared Cu-Co nanosheets.

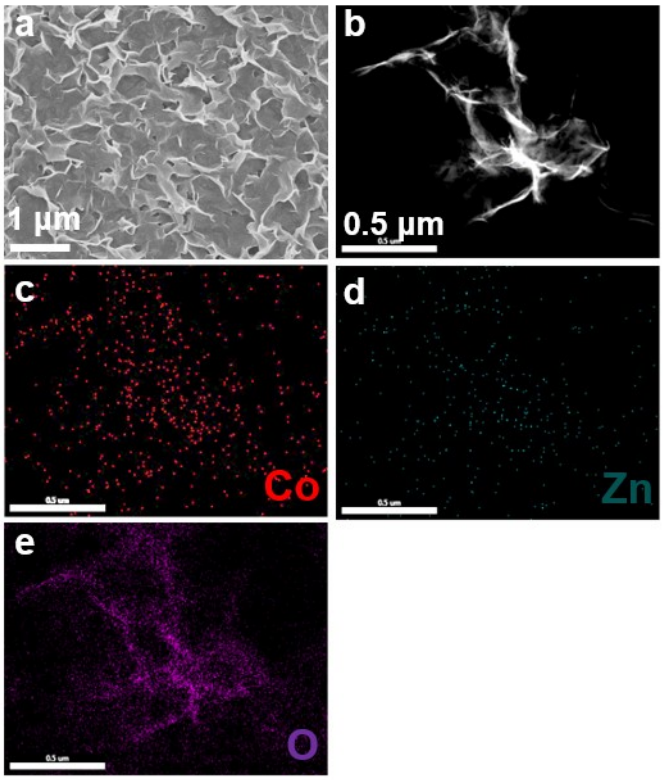

Figure S23. The SEM image (a), HAADF-STEM image (b) and the elemental mapping images (c-e) of the as-prepared Zn-Co nanosheets.

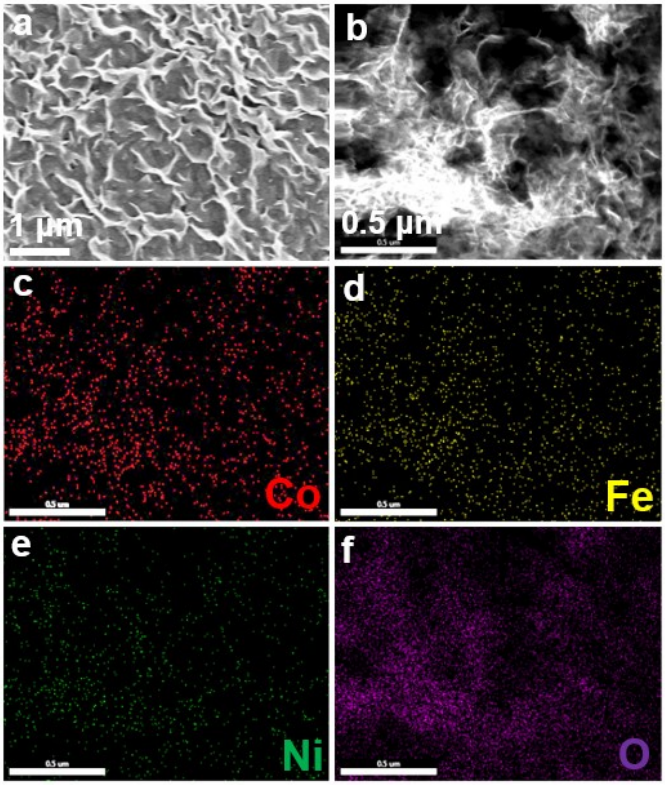

Figure S24. The SEM image (a), HAADF-STEM image (b) and the elemental mapping images (c-f) of the as-prepared Ni-Fe-Co nanosheets.

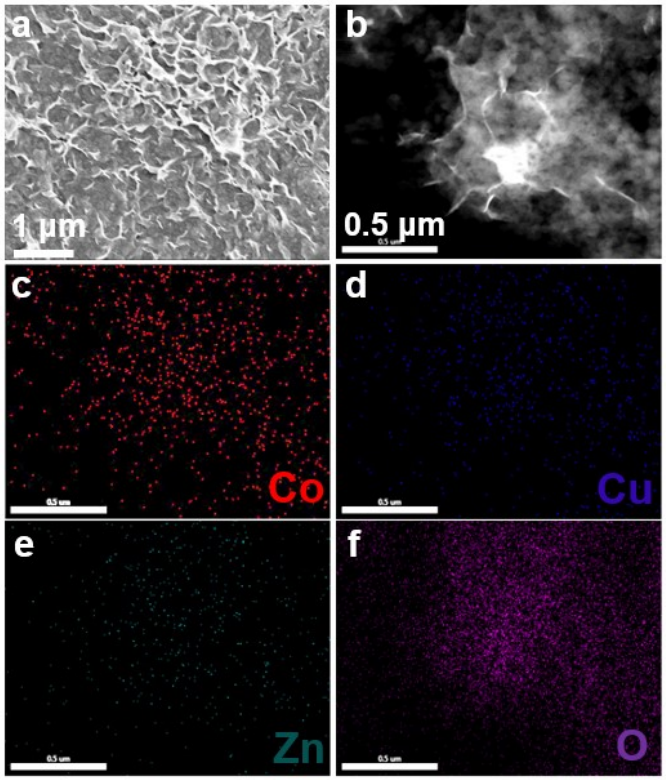

Figure S25. The SEM image (a), HAADF-STEM image (b) and the elemental mapping images (c-f) of the as-prepared Cu-Zn-Co nanosheets.

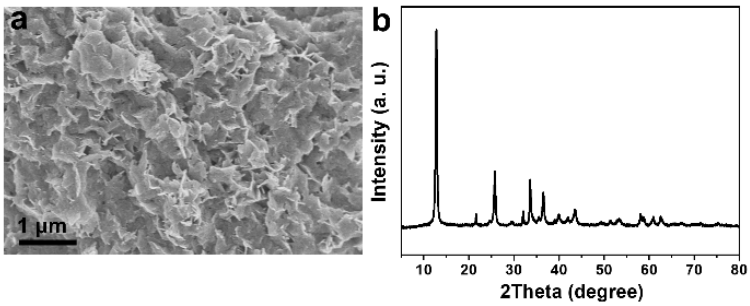

Figure S26. The SEM image and XRD pattern of as-prepared Cu hydroxide nanosheets.

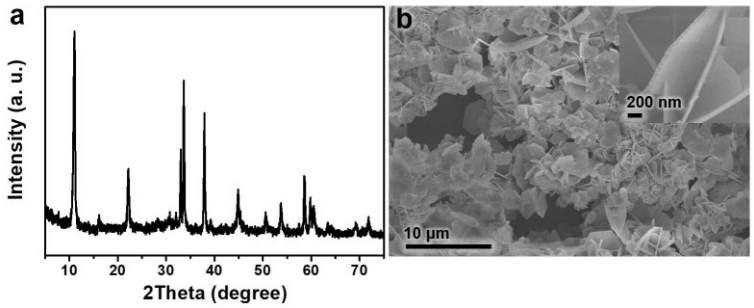

Figure S27. XRD pattern (a) and SEM image (b) of hexagonal α-$Co(OH)_2$ plates

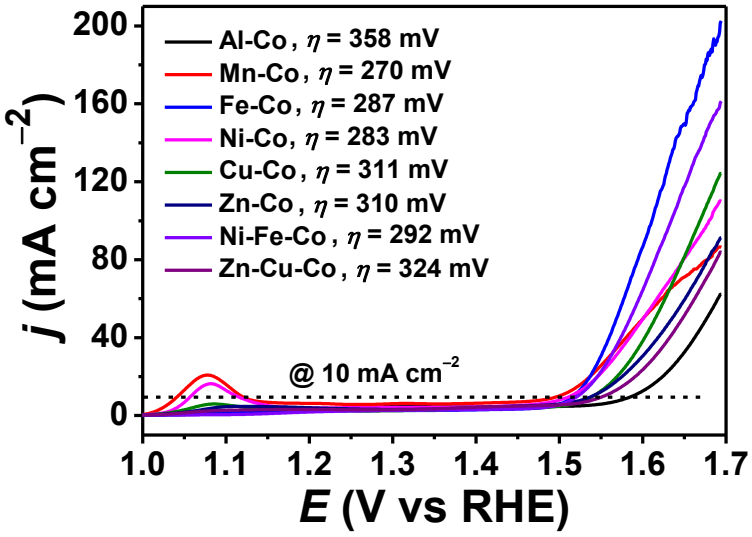

Figure S28. LSV curves of Co-based layered double and triple hydroxides

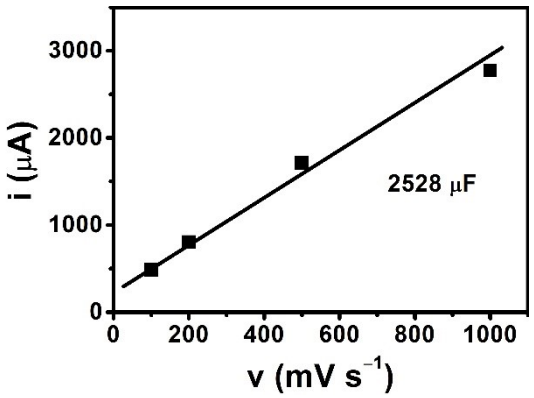

Figure S29. Capacitance currents dependence of scan rates for the α-$Co(OH)_2$ nanosheets.

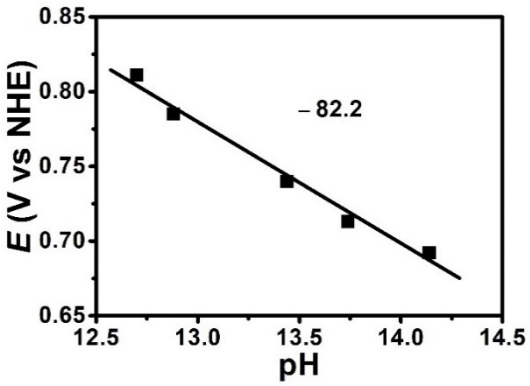

Figure S30. The pH dependence of the potential *E* at a specific current density (10 mA cm^{-2}) for the α-$Co(OH)_2$ nanosheets